

Spin-wave velocity, entropy, and magnetization in bcc solid ³He

W. Ni, J. S. Xia, and E. D. Adams

Department of Physics and Center for Ultralow Temperature Research, University of Florida, Gainesville, Florida 32611

(Received 31 January 1994)

Precise measurements of the ³He melting pressure in several magnetic fields have been made through the various magnetic ordering transitions. Throughout the low-field phase, we find a T^4 temperature dependence of the melting pressure, characteristic of antiferromagnetic spin waves with linear dispersion and a velocity of 7.8 cm/s, almost independent of field. However, the melting pressure in the high-field phase (HFP) deviates from the T^4 dependence near the HFP-paramagnetic phase transition, resulting in a very rapid entropy change near T_c . The spin-wave velocity increases with field, consistent with a strong temperature dependence of the magnetization. The entropy and magnetization discontinuities across the various phase boundaries have been determined. All results are thermodynamically consistent with the measured magnetic phase diagram.

Solid ³He has two magnetically ordered phases near 1 mK (at melting pressure), resulting from multiple atom-atom exchange.^{1,2} The low-field phase (LFP), which exists up to a critical field $B_{c1}=0.45$ T (at $T=0$), has an $u2d2$ configuration of spins.³ The high-field phase (HFP), occurring at higher fields, has a high magnetization^{1,4-6} but no NMR frequency shift, indicating cubic symmetry,^{5,6} with a structure thought to be a canted normal antiferromagnet.⁷ Above an upper critical field, expected at $B_{c2} \approx 20$ T (at $T=0$),^{7,8} the paramagnetic phase (PP), which encircles the HFP, is the stable phase. All transitions are known to be first order, except for the HFP-PP transition, which has recently been shown to be first order below about 0.6 T, above which it is second order.⁹

In this paper we present the results of precise melting pressure measurements over a wide range of temperature, at several magnetic fields, from which we determine the spin-wave velocity, entropy, and magnetization which are thermodynamically consistent with our measured magnetic phase diagram.⁹ Our previous work,^{9,10} in which the experimental arrangement was described, concentrated on only the region near the phase transitions.

The melting pressure is expected to have a T^4 temperature dependence (specific heat $C_v \sim T^3$) for $T \ll T_N$ because of the linear dispersion curve for the low-energy spin-wave excitations. In a recent calculation, Sun and Hetherington¹¹ find $C_v \sim T^3$ only for $T < 40 \mu\text{K}$, with a significant increase in C_v/T^3 at higher T . However, previous low-field measurements of the melting pressure have shown the T^4 dependence up to T_N .¹²

Figure 1 shows the melting pressure versus T^4 at several different fields. In the LFP the T^4 temperature dependence up to the phase transitions can be seen, where, within experimental error, the slopes are independent of field. In contrast, the melting pressure in the HFP deviates from the T^4 dependence near the HFP-PP transition and the slope decreases as the field increases.

In the region of the T^4 dependence, the melting pressure as a function of B and T can be represented by

$$P(T, B) = P(0, B) - a(B)T^4, \tag{1}$$

where $P(0, B)$ is the limiting melting pressure at $T=0$. The spin-wave velocity is related to the prefactor $a(B)$ by

$$v_{\text{spin}} = \left(\frac{n \pi^2 k_B^4 v_s}{90a \Delta v \hbar^3} \right)^{1/3}, \tag{2}$$

where k_B is the Boltzmann constant, $\Delta v = 1.314 \text{ cm}^3/\text{mol}$,² the molar volume change on melting, v_s is the solid ³He molar volume, and n is the number of spin-wave modes. In the LFP $n = 2$ and in the HFP $n = 1$.

Shown in Fig. 2 (open squares) are the spin-wave velocities as a function of field obtained from the melting pressure slopes.

Our results, that v_{spin} is independent of field in the LFP, are in contrast to calculations of Greywall and Busch,¹³ based on scaling of the heat capacity and an assumed

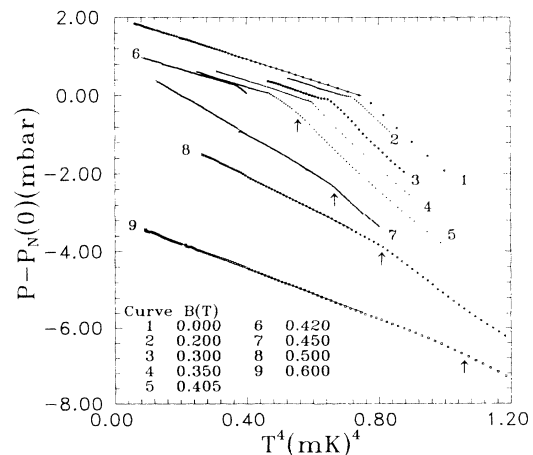


FIG. 1. Melting pressure versus T^4 . Lower temperature portions of curves are 1-6, LFP; 7-9, HFP. Pressure is relative to the LFP-PP transition pressure at zero field $P_N(0)$. The arrows mark the HFP-PP transition.

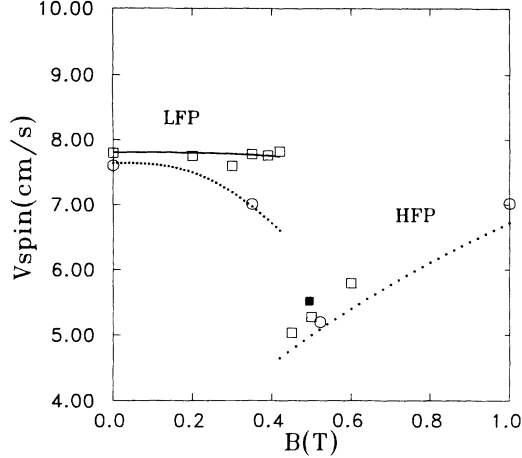


FIG. 2. Spin-wave velocity versus magnetic field. Open circles are from Ref. 8, the dotted lines are from Ref. 13, solid square is Ref. 18, open squares are measured in this work, and the solid line is calculated based on the melting pressure at the LFP-PP transition.

value of the triple-point temperature, $T_t = 880 \mu\text{K}$, where the three phases coexist. The points shown by the circles are derived from the results of Osheroff, Godfrin, and Ruel.⁸ These values are given in Ref. 13, but have not been reported in the original literature.¹⁴ In the HFP, v_{spin} is a function of magnetic field and there is generally good agreement among the various authors.^{8,13,18}

The solid line for the LFP is from a calculation based on our measurement of the triple-point pressure and temperature. If we follow the procedure of Greywall and Busch,¹³ using our measured value of $T_t = 846 \mu\text{K}$,⁸ the calculated v_{spin} is almost independent of field in the LFP, as shown by the solid line in Fig. 2. Here we describe a procedure that uses the phase boundary in the P - B plane for calculating the spin-wave velocity.

We obtain an expression for $P_N(B)$ by substituting into Eq. (1) the equation for the LFP-PP transition temperature as a function of field, found in our previous work,⁹

$$T_N(B) = T_N(0) - \gamma B^2, \quad (3)$$

where $T_N(0) = 0.931 \text{ mK}$, and $\gamma = 0.545 \text{ mK/T}^2$. For $P(0, B)$ we write

$$P(0, B) = P(0, 0) - \frac{\chi B^2}{2\Delta v}, \quad (4)$$

where χ is the magnetic susceptibility at $T=0$. We find $\chi = 1.3 \times 10^{-4} \text{ mol}^{-1}$ for the LFP from $P(0, B)$, in good agreement with the value of Osheroff, Godfrin, and Ruel.⁸ Following Greywall and Busch,¹³ we write $a(B) = a_0 + a_1 B^3$, where we find $a_0 = 2.65 \text{ mbar}/(\text{mK})^4$. Then subtracting $P_N(0)$ from $P_N(B)$, we have

$$P_N(0) - P_N(B) = \frac{\chi B^2}{2\Delta v} - a_0 T_N^4(0) + [a_0 + a_1 B^3][T_N(0) - \gamma B^2]. \quad (5)$$

Our measured points for the melting pressure at various phase transitions versus B are shown in Fig. 3. We

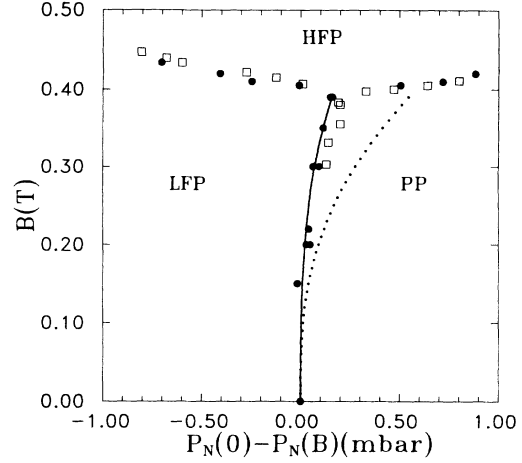


FIG. 3. Magnetic field versus melting pressure B - P phase diagram of solid ^3He . Open squares are from Ref. 19, the dotted line is calculated from Greywall and Busch's $a_1 = 13.5$ (Ref. 13), solid circles are from this work, and the solid line is a least-squares fit with $a_1 = 0.9$.

solve for a_1 using the least-squares fit to these points and find $a_1 = 0.9$, which gives $a_1 B^3$ equal to only 3% of a_0 for $B = 0.45 \text{ T}$. The spin-wave velocity calculated using $a_1 = 0.9$ is shown in Fig. 2 (solid line). The implication of the field-independent v_{spin} for the magnetization will be discussed later.

The entropy of the solid, obtained from dP/dT through the Clausius-Clapeyron equation using $\Delta v = 1.314 \text{ cm}^3/\text{mol}$ and $S_1 \approx 0$, is shown in Fig. 4 for various fields. In the region of T^4 dependence of the melting pressure [see Eq. (1)], the entropy has a T^3 dependence, which can be written as

$$S(T, B) = 4a(B)\Delta v T^3. \quad (6)$$

In the LFP, $a(B) \approx a_0$, and the entropy is essentially field independent. The entropy in the HFP can still be

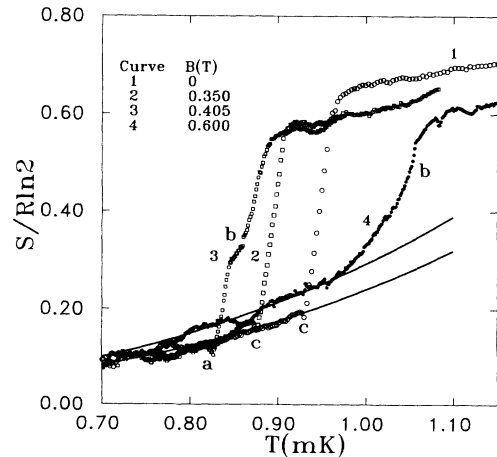


FIG. 4. Entropy versus temperature at several fields. Lower temperature portions of curves are 1-3, LFP; 4, HFP. The LFP-HFP, HFP-PP, and the LFP-PP transitions are marked by a , b , and c respectively. Solid smooth lines are T^3 fits.

represented by Eq. (6), except very near the HFP-PP transition where it rises more rapidly than T^3 . In contrast to the LFP, $a(B)$ is now a function of B [see Fig. 1 and Eq. (1)]. The entropy has a strong field dependence, consistent with the temperature dependence of the magnetization, to be discussed below. (Note that the curve for $B=0.405$ T has portions in both LFP and HFP.)

In the PP, for $T < 3$ mK, our entropies can be represented quite well by

$$S(T, B) = S(T, 0) - \frac{bR \ln 2}{2} \left(\frac{B}{T} \right)^2, \quad (7)$$

where $b = 0.58$ (mK/T)² and R is the gas constant. This is consistent with Greywall and Busch's heat capacity¹³ and the Curie-law behavior of the magnetization, given by

$$M(T) = b \left(\frac{B}{T} \right) R \ln 2, \quad (8)$$

which has been observed by a number of workers.^{15,16} We use this expression for S in the PP along with Eq. (6) for the LFP and HFP to calculate the smooth family of curves for $S(T, B)$ shown in Fig. 5.¹⁷ These are entirely consistent with our values obtained from dP/dT , however, for clarity we have not superposed the two. The entropy obtained from Sun and Hetherington's specific-heat calculation is shown by the dashed line. This departs sharply from our measurements and is about 50% above our value near T_N . While departure of the specific heat from the T^3 behavior would be challenging to detect experimentally, the effect would be easily seen in the entropy given by $\int C_v T^{-1} dT$.

The field dependence of the entropy difference across the LFP-PP transition is shown in Fig. 6 (along with the magnetization difference, to be discussed later). The squares are individually measured points from dP/dT ,

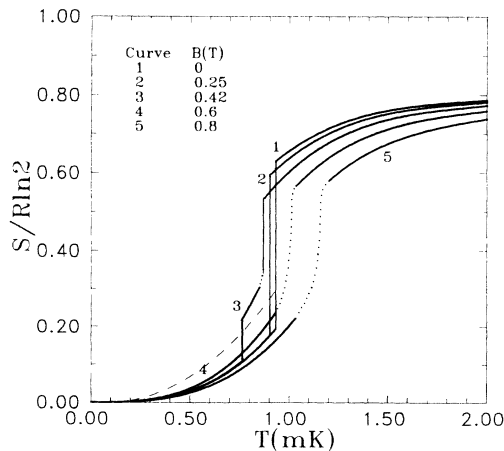


FIG. 5. Family of curves of entropy versus temperature based on Eqs. (6) and (7). Near the HFP-PP transition these lines are joined smoothly by the dotted section, based on the experimental results. The dashed line is calculated from Sun and Hetherington's specific-heat calculation (Ref. 10). Lower temperature portions of curves are 1–3, LFP; 4–5, HFP.

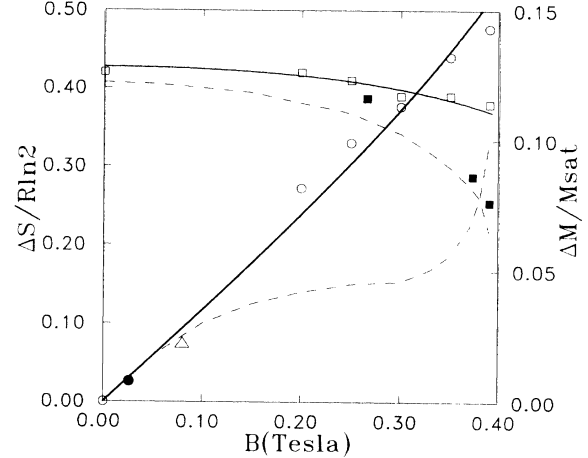


FIG. 6. Entropy and magnetization discontinuities across the LFP-PP transition. The dashed lines are from Ref. 13, solid squares are from Ref. 18, solid circle is from Ref. 16, open triangle is from Ref. 15, open squares and circles are from this work, the solid lines are calculated [see text].

while the solid line is the calculated value from the expressions for S in the PP and LFP and Eq. (3), given above. The entropy discontinuity ΔS versus B shows only weak field dependence for the LFP-PP transition. This is primary because of the lack of B dependence of S in the LFP. The dashed line calculated by Greywall and Busch¹² and the measurements of Tang, Adams, and Uhlig¹⁸ show a much stronger field dependence than we find.

The temperature dependence of the magnetization is related to the field dependence of the entropy through the Maxwell relation

$$\left(\frac{\partial M}{\partial T} \right)_B = \left(\frac{\partial S}{\partial B} \right)_T. \quad (9)$$

We substitute the expression for $S(T, B)$ from Eq. (6) and integrate over T to obtain $M(T, B)$. In the LFP or HFP, where the T^4 temperature dependence of the melting pressure is valid, the magnetization can be expressed as

$$M(T, B) = M(0, B) + \Delta v T^4 \left[\frac{da(B)}{dB} \right], \quad (10)$$

where $M(0, B) = \chi B$ is the magnetization at $T=0$. For the LFP we use χ obtained from this work; for the HFP we use χ from Ref. 8, since it is obtained using a much wider range of field.

In the LFP, since $a(B)$ was found to be almost field independent, Eq. (10) shows that $M(T, B)$ is almost temperature independent. Calculations of $M(T, B)$ from Eq. (10) using $a_1 = 0.9$ are shown in Fig. 7. The data of Hata *et al.* for $B = 0.026$ T are consistent with our results. Reliable measurements of $M(T, B)$ at higher fields are not available for comparison with our calculation. Our results, which follow directly from the field-independent melting pressure slope and spin-wave velocity, are in contrast to the calculation of Greywall and Busch who found a strong T dependence at higher fields in the LFP.

In the HFP, $a(B)$ is a function of B , which, from Eq. (10) gives a T^4 temperature dependent magnetization. Near the HFP-PP transition, the magnetization drops faster than T^4 because of the deviation of the melting pressure from the T^4 temperature dependence. The smooth family of curves for $M(T, B)$, shown in the Fig. 7, is based on the Eqs. (8) and (10) as discussed above.¹⁷

The magnetization discontinuity ΔM across the LFP-PP transition may be obtained from the magnetic Clausius-Clapeyron equation,

$$\frac{dT_N(B)}{dB} = -\frac{\Delta M}{\Delta S}, \quad (11)$$

using ΔS of this work and $T_N(B)$ from Ref. 9. The results are shown in Fig. 6, where the circles are individual points obtained in this work. We find that ΔM is essentially linear in B , which follows from $\Delta S \approx \text{const}$ and $T_N \sim B^2$. The solid line is calculated from Eqs. (8) and (10), using $T_N(B)$ from Ref. 9. This line has an upward curvature caused by the lower value of $T_N(B)$ with increasing B entering into $M(T, B)$ in Eq. (8). The dashed line calculated by Greywall and Busch¹³ shows a quite different behavior.

In conclusion, in the LFP we have found a T^4 slope for the melting pressure, almost field independent, indicative of a constant spin-wave velocity of 7.8 cm/s and a temperature-independent magnetization. Different conclusions have been obtained based on scaling of the heat capacity and an assumed triple-point temperature considerably higher than ours. Our values for the entropy in the LFP near T_N are inconsistent with an increase in C_v above the T^3 dependence found in recent calculations. In the HFP, we find a field-dependent spin-wave velocity and a strongly temperature-dependent magnetization

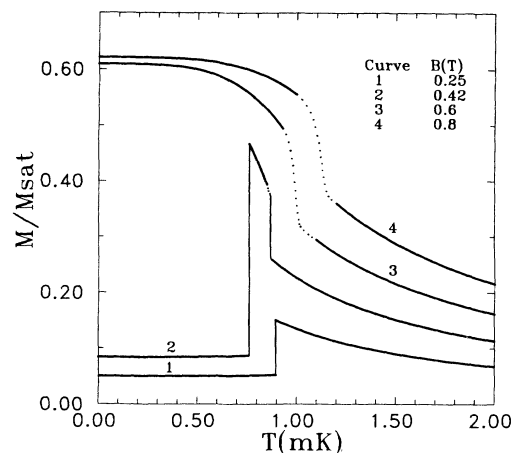


FIG. 7. Family of curves of magnetization versus temperature based on Eqs. (8) and (10). Near the HFP-PP transition these lines are joined smoothly by the dotted section based on the experimental results. Lower temperature portions of curves are 1–2, LFP; 3–4, HFP.

similar to that of other workers. The present results are thermodynamically consistent with our earlier determination of the phase diagram.

This work was supported by the National Science Foundation, Low Temperature Physics, Grant No. DMR-9019736. We thank Professor N. Sullivan, Professor Y. Takano, and Professor P. Kumar for useful discussions, and G. Labbe and B. Lothop for supplying liquid helium during this extended experiment.

¹R. B. Kummer, R. M. Mueller, and E. D. Adams, *J. Low Temp. Phys.* **27**, 319 (1977).

²W. P. Halperin, F. B. Rasmussen, C. N. Archie, and R. C. Richardson, *J. Low Temp. Phys.* **31**, 617 (1978).

³D. D. Osheroff, M. C. Cross, and D. S. Fisher, *Phys. Rev. Lett.* **44**, 792 (1980).

⁴T. C. Prewitt and J. M. Goodkind, *Phys. Rev. Lett.* **39**, 1283 (1977).

⁵D. D. Osheroff, *Physica* **109 & 110B**, 1461 (1982).

⁶E. D. Adams, E. A. Shubert, G. E. Haas, and D. M. Bakalyar, *Phys. Rev. Lett.* **44**, 789 (1980).

⁷M. Roger, J. H. Hetherington, and J. M. Delrieu, *Rev. Mod. Phys.* **55**, 1 (1983).

⁸D. D. Osheroff, H. Godfrin, and R. R. Ruel, *Phys. Rev. Lett.* **58**, 2458 (1987).

⁹J. S. Xia, W. Ni, and E. D. Adams, *Phys. Rev. Lett.* **70**, 1481 (1993).

¹⁰J. S. Xia, W. Ni, and E. D. Adams, *J. Low Temp. Phys.* **89**, 355 (1992).

¹¹Z. Sun and J. H. Hetherington, *J. Low Temp. Phys.* **90**, 355 (1993).

¹²D. D. Osheroff and C. Yu, *Phys. Lett.* **77A**, 458 (1980).

¹³D. S. Greywall and P. A. Busch, *Phys. Rev. B* **36**, 6853 (1987).

¹⁴Osheroff *et al.* were concerned with the limiting pressure as $T \rightarrow 0$ and did not have a high-field thermometer needed to obtain the melting pressure slope. D. D. Osheroff (private communication).

¹⁵T. C. Prewitt and J. M. Goodkind, *Phys. Rev. Lett.* **44**, 1699 (1980).

¹⁶T. Hata, S. Yamasaki, T. Kodama, and T. Shigi, *J. Low Temp. Phys.* **71**, 193 (1988).

¹⁷Near the HFP-PP transition, the curves are joined smoothly (dotted section) based on our experimental results.

¹⁸Y. H. Tang, E. D. Adams, and K. Uhlig, *Phys. Rev. Lett.* **57**, 222 (1986).

¹⁹T. Okamoto, H. Fukuyama, T. Fukuda, H. Ishimoto, and S. Ogawa, *Physica B* **165 & 166**, 825 (1990).